# Explicit Nonlinear Model Predictive Control for Electric Vehicle Traction Control

Davide Tavernini , Mathias Metzler , *Graduate Student Member, IEEE*,
Patrick Gruber , and Aldo Sorniotti , *Member, IEEE*

*Abstract*—This paper presents a traction control (TC) system for electric vehicles with in-wheel motors, based on explicit nonlinear model predictive control. The feedback law, available beforehand, is described in detail, together with its variation for different plant conditions. The explicit controller is implemented on a rapid control prototyping unit, which proves the real-time capability of the strategy, with computing times on the order of microseconds. These are significantly lower than the required time step for a TC application. Hence, the explicit model predictive controller can run at the same frequency as a simple TC system based on proportional integral (PI) technology. High-fidelity model simulations provide: 1) a performance comparison of the proposed explicit nonlinear model predictive controller (NMPC) with a benchmark PI-based traction controller with gain scheduling and anti-windup features, and 2) a performance comparison among two explicit and one implicit NMPCs based on different internal models, with and without consideration of transient tire behavior and load transfers. Experimental test results on an electric vehicle demonstrator are shown for one of the explicit NMPC formulations.

*Index Terms*—Electric vehicle, in-wheel motors, model predictive control (MPC), proportional integral (PI) control, traction control (TC), wheel slip.

## I. INTRODUCTION

**T**HE adoption of electric drivetrains, and in particular of in-wheel motor layouts, has the potential of significantly enhancing the performance of wheel slip control systems, i.e., antilock braking systems (ABS) and traction control (TC) systems [1]. This is caused by the higher control bandwidth and precision in torque modulation that electric drivetrains can offer, with respect to the more conventional internal combustion engines and hydraulic/electro-hydraulic braking units. Murata [2] and Ivanov *et al.* [3] include experimentally measured reductions in stopping distances and acceleration times, achieved through the continuous modulation of the electric drivetrain torques. However, further work can be done in terms of control design to enhance the slip ratio tracking performance and the seamless blending of the regenerative and dissipative braking contributions.

In parallel to sliding mode control [4] and maximum transmissible torque estimation [5] algorithms, the recent literature (see [6]–[18]) on the topic of ABS and TC shows growing interest in model-based control, with focus on model predictive control (MPC). For example, [6] discusses a gain scheduled linear quadratic regulator approach for ABS control, with experimental results on an internal-combustion-engine-driven vehicle with electro-mechanical brakes. Boisvert *et al.* [7] and Anwar and Ashrafi [8] include different approaches to ABS control, i.e., linear quadratic Gaussian regulation and generalized predictive control, which is reproposed in [9] for a TC implementation. A linear MPC strategy is developed in [10], where the ABS slip regulation is achieved through torque blending between the friction brakes and in-wheel motors. Similarly, [11]–[13] combine ABS control and torque blending, by using linear MPC formulations. Yoo and Wang [14] present an MPC-based ABS, with test results on a hardware-in-the-loop rig. The internal model includes a tire force dynamics formulation; however, its effect on the controller performance is not discussed in this paper, nor, to the authors' knowledge, in any other study in the literature. Yuan *et al.* [15] present a nonlinear model predictive controller (NMPC) for ABS and TC. The formulation considers all four wheels in the same internal model. Reference tracking is not used, since the slip ratio is solely controlled through the constraints of the NMPC formulation. Moreover, the tire-road friction coefficient is considered to be known *a priori*, which introduces some challenges for a real vehicle implementation. For an internal-combustion-engine-driven vehicle, [16] introduces four linear MPC TC strategies that are compared with a hybrid explicit MPC. The hybrid design adopts a piecewise linear approximation of the nonlinear longitudinal tire force characteristic as a function of the slip ratio. Simulation and experimental results show the performance enhancement of the hybrid strategy with respect to the linear approaches.

In the case of implicit NMPC, a nonlinear programming (NLP) problem is solved on-line at each sampling time. The resulting computational load makes implicit NMPC difficult to implement in real automotive applications, if the required sampling frequency is high. In this respect, Basrah *et al.* [17] provide an example of real-time capable NMPC for an ABS with torque blending, including a comparison with a linear MPC approach. The results show that the

computational time of the implicit NMPC, i.e., 3–4 ms on a desktop personal computer, is within the selected time step of 5 ms. In [15], the implicit NMPC strategy is run on a rapid control prototyping unit, with a computational time of 4–5 ms and an implementation time step of 10 ms.

The study of this paper presents an explicit NMPC (eNMPC in the remainder) for TC on electric vehicles with in-wheel drivetrains. The explicit solution is computed off-line by using a multiparametric (mp) quadratic programming (QP) approximation of the mp-NLP problem. The control action is evaluated on-line at each sampling time starting from the current values of system states and parameters, and the off-line explicit solution, stored in the memory of the control unit. This drastically reduces the required computational load. The other advantage is that the complete feedback law is available beforehand in its explicit form, which allows its analysis for the range of states and reference parameters.

Another important aspect is the performance comparison and critical analysis of different TC implementations. In this respect, [16] claims that the performance of the proposed MPC "is comparable with that of a well-tuned PID" controller. The same authors state that "the simulation and test results demonstrated that the $l_1$-optimal hybrid controller used in this problem can lead to about 20% reduction in peak slip amplitudes and corresponding spin duration when compared to best case linear MPC counterparts." Similarly, [17] shows the superiority of NMPC over linear MPC in terms of slip control performance. The necessity of "objective benchmarking technologies" in the field of ABS/TC was pointed out in the survey study in [19]. In order to understand where the strategies of different papers stand with respect to each other, a comparison is well needed. De Pinto *et al.* [20] partially cover this knowledge gap, but limit the analysis to on-board electric drivetrains, characterized by significant torsional dynamics. Satzger and de Castro [13] include also an MPC-PI experimental comparison, but for an ABS application combined with torque blending.

Based on the previous discussion, the points of novelty of this paper are as follows.

1) The design of TC systems based on explicit NMPC, implementable at the same time step as a typical PI controller for TC, but with better tracking performance.
2) The study of the explicit feedback control law, and its dependency on the vector of parameters from the plant.
3) The simulation-based analysis of the performance advantages of the proposed eNMPC compared to a well-tuned benchmark PI TC system with gain scheduling and anti-windup features.
4) The sensitivity analysis of the performance of TC algorithms with respect to their time step.
5) The discussion of the benefit of considering transient tire response and vertical load transfers in the internal model for the NMPC formulation.
6) The presentation of experimental test results based on explicit NMPC applied to a fully electric vehicle prototype with in-wheel drivetrains.

## II. EXPLICIT NONLINEAR MODEL PREDICTIVE CONTROL

### A. Problem Formulation

Similarly to the NMPC, the explicit NMPC requires the formulation of an optimization problem, potentially including constraints on the control inputs and system states. A generic nonlinear optimal control problem for a finite horizon in the time interval $[t_k, t_f]$ can be defined as the minimization of the following cost function:

$$V(x[t_k, t_f], u[t_k, t_f], p(t_k), v[t_k, t_f])$$
$$\triangleq \int_{t_k}^{t_f} L(x(t), u(t), p(t_k), v(t))dt + M(x(t_f), p(t_k), t_f) \tag{1}$$

where $x$, $u$, $p$, and $v$ are the state, input, parameter, and slack variable vectors, respectively. $L$ is the stage cost, and $M$ is the terminal cost. The problem is subject to inequality constraints of the form

$$x_{\min} \leq x(t) \leq x_{\max} \tag{2}$$
$$u_{\min} \leq u(t) \leq u_{\max} \tag{3}$$
$$g(x(t), u(t), p(t_k), v(t), t) \leq 0. \tag{4}$$

The ordinary differential equations (ODEs) describing the system dynamics represent the equality constraints:

$$\frac{d}{dt}x(t) = f(x(t), u(t), p_s(t_k), t) \tag{5}$$

where $p_s$ is the vector of the system parameters. The initial conditions $x(t_k)$ are assigned to the state vector.

The infinite-dimensional optimal control problem in (1)–(5) is discretized and parametrized, thus becoming an NLP problem, which is solved through numerical methods. This approach is known as direct method [21]. In this operation, the equality constraints (5) are represented as finite approximations. The infinite-dimensional unknown solution, $u[t_k, t_f]$, and the slack variables, $v[t_k, t_f]$, are replaced by a finite number of decision variables. The prediction horizon $t_p = t_f - t_k$ is defined as $t_p = N_p t_s$, where $N_p$ is the number of prediction steps and $t_s$ is the characteristic discretization interval of the internal model. The input signal, $u[t_k, t_f]$, is assumed to be piecewise constant along the horizon. It is calculated through the function $\chi$ and is parameterized through the vector of control parameters $U$ such that $u(t) = \chi(t, U)$. Similarly, the piecewise constant slack variable trajectory is parameterized through the vector of slack variables, $N$.

The technique known as direct single shooting (see [21], [22]) is used for the management of the equality constraints. It consists of eliminating the ODE equality constraints by substituting their discretized numerical solution into the cost function and constraint formulations. Starting from the continuous constraint equations (5), the numerical solution is derived by discretization and integration of the ODEs

$$x(t_{k+j}) = \phi(x(t_k), U, p_s(t_k), t_{k+j}), \quad j = 1, \ldots, N_p. \tag{6}$$

To obtain the function $\phi$, an explicit integration scheme is selected

$$x(t_{k+j+1}) = F(x(t_{k+j}), \chi(t_{k+j}, U), p_s(t_k), t_{k+j}) \tag{7}$$

with given initial conditions $x(t_k)$. If the whole horizon is considered, the state trajectories are all mapped into a single function, and the system dynamics do not appear any more as equality constraints

$$x(t_{k+j}) = F(x(t_{k+j-1}), \chi(t_{k+j-1}, U), p_s(t_k), t_{k+j-1})$$

$$= F(F(\dots \underbrace{F(\underbrace{F(\underbrace{x(t_k), \dots, t_k)}_{x(t_{k+1})}, \dots, t_{k+1})}_{x(t_{k+2})}, \dots, t_{k+j-2}), \dots, t_{k+j-1})}_{x(t_{k+j-1})}.$$

$$(8)$$

The optimal control problem is now in its generic mp-NLP form

$$V^*(x(t_k), p(t_k)) = \min_{U,N} V(x(t_k), U, p(t_k), N) \qquad (9)$$

subject to

$$G(x(t_k), U, p(t_k), N) \le 0 \qquad (10)$$

where $p$ includes the system and controller parameters, which are considered constant for the duration of the prediction horizon. Two additional vectors are defined: 1) the vector of parameters $x_p(t_k) \in \mathbb{R}^{n_p}$, where $n_p = n + d$, i.e., $n_p$ is the sum of the number of states $n$ and the number of parameters $d$

$$x_p(t_k) = \begin{bmatrix} x(t_k) \\ p(t_k) \end{bmatrix} \qquad (11)$$

and 2) the vector of decision variables, $z \in \mathbb{R}^s$

$$z = \begin{bmatrix} U \\ N \end{bmatrix}. \qquad (12)$$

Based on (11) and (12) it is possible to reformulate the optimization problem as

$$V^*(x_p(t_k)) = \min_z V(z, x_p(t_k)) \qquad (13)$$

$$\text{s.t. } G(z, x_p(t_k)) \le 0. \qquad (14)$$

The minimization is performed with respect to $z$ and is parameterized with $x_p(t_k)$.

### B. Off-Line Solution

The mp-NLP problem is not solved directly, but through its approximation (see [23]). In this paper, an mp-QP formulation is adopted, as suggested in [21] and implemented in [24]. The mp-NLP in (13) and (14) is linearized around a predefined point $(z_0, x_{p,0})$ by means of Taylor series expansion (with $z_0$ being the optimal solution at $x_{p,0}$), such that the cost function is approximated with a quadratic function (15)–(16) and the constraints assume a linear

formulation (17)

$$V_0(z, x_p) \triangleq \frac{1}{2}(z - z_0)^T H_0(z - z_0)$$
$$+ (D_0 + (x_p - x_{p,0})^T F_0)(z - z_0) + Y_0(x_p) \qquad (15)$$

$$Y_0(x_p) \triangleq \frac{1}{2}(x_p - x_{p,0})^T \nabla^2_{x_p x_p} V(z_0, x_{p,0})(x_p - x_{p,0})$$
$$+ (\nabla_{x_p} V(z_0, x_{p,0}))^T (x_p - x_{p,0}) + V(z_0, x_{p,0}) \qquad (16)$$

$$G_0(z - z_0) \le E_0(x_p - x_{p,0}) + T_0. \qquad (17)$$

The different terms are computed as follows and evaluated at the linearization point $(z_0, x_{p,0})$:

$$H_0 \triangleq \nabla^2_{zz} V(z_0, x_{p,0})$$
$$D_0 \triangleq (\nabla_z V(z_0, x_{p,0}))^T$$
$$G_0 \triangleq (\nabla_z G(z_0, x_{p,0}))^T$$
$$E_0 \triangleq -(\nabla_{x_p} G(z_0, x_{p,0}))^T$$
$$T_0 \triangleq -G(z_0, x_{p,0})$$
$$F_0 \triangleq \frac{1}{2}((\nabla^2_{zx_p} V(z_0, x_{p,0}))^T + \nabla^2_{x_p z} V(z_0, x_{p,0})). \qquad (18)$$

The mp-QP formulation is employed to compute local approximations of the original mp-NLP problem in the exploration space. This is represented as a number of hyper-rectangles, on which single mp-QP problems are solved. Each hyper-rectangle is further partitioned into poly-hedra, i.e., the critical regions for the mp-QP problem. Finally, the mp-QP solution is represented as a piecewise affine function that is continuous across the boundaries among different polyhedra, but discontinuous across the hyper-rectangles.

In this paper, the mp-QP problems are computed by means of Multi-Parametric Toolbox 3.0 [25]. The solution is evaluated in points of interest within each hyper-rectangle and compared with the solution of the NLP problem at the same points, where the initial state conditions are the coordinates of the points themselves. The NLPs are computed by means of IPOPT, a software package for nonlinear optimization [26]. Based on the maximum error between the evaluated mp-QP and computed NLP solutions for all the points, a decision is made whether to subpartition the hyper-rectangle into smaller ones, or to stop the process and accept the mp-QP approximating solution. The algorithm in [21] that implements this concept is summarized. For all the unexplored hyper-rectangles the following steps are implemented.

1) Compute the hyper-rectangle volume. (A minimum volume is defined to decide whether the hyper-rectangle can be further split.)
2) Compute the NLP solution (or recover it from previous steps) at the points of interest.
3) Compute the mp-QP solution on the whole hyper-rectangle, using the NLP solution at the Chebyshev center plus its coordinates, as the linearization point for the terms in (15)–(18).

4) Evaluate the mp-QP solution for all the aforementioned points.
5) Calculate the maximum error between the NLP-computed solutions and the mp-QP-evaluated solutions.

Based on this information each hyper-rectangle is either stored or marked "to be split" with a heuristic splitting rule similar to the one in [21]. When all the tolerances are fulfilled or the minimum allowed volume has been reached, the algorithm terminates and the solution is available for any point inside each hyper-rectangle.

With respect to the stability of the resulting controller, common schemes in the literature for implicit MPC include stabilizing terminal constraints or terminal costs, which need to satisfy Lyapunov function-type conditions (see [27], [28]). Alternatively, Grüne [29], and Reble and Allgöwer [30] present a stability and performance analysis technique for unconstrained (with respect to stability preserving constraints) implicit NMPC schemes. However, all these approaches are for implicit cases. To the best of the authors' knowledge, there is no comparable practical NMPC theory in the literature addressing the stability for explicit NMPC. Therefore, in this paper the eNMPC stability will be verified empirically through the simulated scenarios and experimental test results of Sections V and VI.

### C. Implementation of the Explicit Solution for Real-Time Applications

Once the solution is computed off-line, the next step is to define the most efficient way to access it on-line. This is performed through point location and piecewise control function evaluation. In particular, the former problem becomes challenging if the total number of regions composing the final solution is large (>1000–2000). Two families of methods are available.

1) Sequential search methods, which, in the worst case, may check every region to identify the one containing the considered point and
2) Binary-search-tree methods [31], providing a fast solution for the location of the point with a limited number of mathematical operations, which is logarithmic in the number of regions, for a balanced tree. As a drawback, binary-search-tree methods require significant off-line processing, which makes them unsuitable for a large number of regions [31].

The specific application (i.e., the 4-D case of Section III-B) has a total number of 85 hyper-rectangles, obtained with the selected approximation tolerances for the values of the cost function, the normalized solution and the maximum normalized constraint violation. A two-layer solution is proposed. The top layer includes a binary-search-tree to determine the index of the hyper-rectangle the measured/estimated point lies in. This information is then passed to the bottom layer, consisting of functions, one for each hyper-rectangle, which identify the correct critical region within the hyper-rectangle, and evaluate the piecewise control function. In the bottom layer either binary-search-tree or sequential search methods can be used, as the number of polyhedral critical regions is

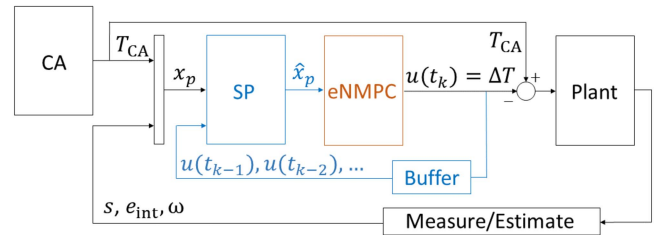| Symbol | Description | Value | Unit |
|--------|-------------|-------|------|
| $m$ | Quarter car mass | 112.5 | kg |
| $r$ | Wheel rolling radius | 0.279 | m |
| $J_w$ | Wheel mass moment of inertia | 1.5 | kgm² |
| $B$ | MF coefficient: stiffness factor | 40 | - |
| $C$ | MF coefficient: shape factor | 1.4 | - |
| $D$ | MF coefficient: peak value | 0.45 | - |
| $F_z$ | Tire vertical load | 1104 | N |
| $\sigma_x^{ref}$ | Slip ratio reference value | 0.10 | - |
| $\sigma$ | Longitudinal relaxation length (*) | 0.200 | m |

(*) 5-D problem only



Fig. 1. Simplified architecture of the implemented TC strategy.

usually limited (i.e., <100 for this TC application), which makes both methods viable in terms of processing burden and searching time.

## III. TRACTION CONTROL DESIGN

This section discusses the structure and formulation of the proposed model predictive TC strategies, first by deriving the internal model, and then by formulating the optimal control problem. In particular, three internal models with increasing complexity are proposed and used with the same cost function and constraints.

The values of the main vehicle data used for internal model parameterization are reported in Table I. They refer to the electric vehicle simulated in Section V.

### A. Traction Control Structure

Fig. 1 shows the TC structure. The torque-vectoring controller of the electric vehicle calculates the total reference wheel torque and the reference yaw moment. The control allocation (CA) algorithm outputs the individual wheel torques for the in-wheel motors, indicated as $T_{CA}$, to achieve the references. A state predictor (SP) compensates for the system delays on the states, e.g., caused by the CAN bus. The predicted parameter vector with the updated states, $\hat{x}_p$, is provided to the core block of the TC, i.e., the on-line implementation of the eNMPC, which outputs the torque correction $\Delta T$, to be subtracted from $T_{CA}$.

### B. 4-D Problem: Internal Model

The controlled variable is the wheel slip velocity $s$

$$s = \omega r - V \tag{19}$$

where $\omega$ is the angular wheel speed, $r$ is the rolling radius of the wheel, and $V$ is the linear speed of the vehicle, so that the

slip ratio is

$$\sigma_x = \frac{\omega r - V}{\omega r} = \frac{s}{\omega r}. \tag{20}$$

The time derivative of (19) is given by

$$\frac{d}{dt}s(t) = r\frac{d}{dt}\omega(t) - \frac{d}{dt}V(t). \tag{21}$$

The first term on the right-hand side results from the wheel moment balance

$$\frac{d}{dt}\omega(t) = \frac{1}{J_w}(T_{CA} - \Delta T(t) - F_x r) \tag{22}$$

where $J_w$ is the wheel mass moment of inertia. $T_{CA}$ is kept constant over the prediction horizon, and thus is a system parameter. $F_x$ is the longitudinal tire force, estimated through a simplified version of the Pacejka magic formula (MF) [33]

$$F_x = \mu_x F_z \tag{23}$$
$$\mu_x = D \sin(C \arctan(B\sigma_x)) \tag{24}$$

where $F_z$ is the vertical tire load, considered as a constant, and $\mu_x$ is the longitudinal tire force coefficient, with $B$, $C$, and $D$ being the MF parameters [33]. The longitudinal vehicle dynamics are modeled by considering a mass $m$ equal to a quarter of the total vehicle mass

$$\frac{d}{dt}V(t) = \frac{1}{m}F_x. \tag{25}$$

By substituting (22) and (25) into (21) the wheel slip dynamic equation, i.e., the first equation of the internal model, is obtained

$$\frac{d}{dt}s(t) = \left(-\frac{r^2}{J_w} - \frac{1}{m}\right)D\sin\left(C\arctan\left(\frac{Bs(t)}{\omega(t)r}\right)\right)F_z + \frac{(T_{CA} - \Delta T(t))r}{J_w}. \tag{26}$$

An integral action is incorporated to tackle the steady-state error and model uncertainties. This considers the integral of the error $e_{int}$ between the actual slip velocity $s$ and the reference slip velocity computed from the target value $\sigma_x^{ref}$ of the slip ratio. The respective differential equation, i.e., the second equation of the internal model, is

$$\frac{d}{dt}e_{int}(t) = s(t) - \sigma_x^{ref}\omega(t)r. \tag{27}$$

By substituting (23) and (24) into (22), the third equation of the internal model is obtained

$$\frac{d}{dt}\omega(t) = \frac{1}{J_w}\left(T_{CA} - \Delta T(t) - D\sin\left(C\arctan\left(\frac{Bs(t)}{\omega(t)r}\right)\right)F_z r\right). \tag{28}$$

The model state vector, input vector and parameter vector are, respectively, $x = [s, e_{int}, \omega]$, $u = [\Delta T]$ and $p = [T_{CA}]$. Unless otherwise specified, in the following analyses the explicit solution is reported for $N_p = 4$ and $t_s = 2$ ms. The parametric problem includes four parameters (4-D problem), i.e., $x_p = [s(t_k), e_{int}(t_k), \omega(t_k), T_{CA}(t_k)]$, and five decision variables, i.e., $z = [\Delta T(t_k), \Delta T(t_{k+1}), \Delta T(t_{k+2}), \Delta T(t_{k+3}), \nu(t_k)]$. The receding horizon control input that is applied to the system is $u(t_k) = \Delta T(t_k)$, which will be

indicated as $u$ in the remainder. The 4-D eNMPC will be referred to as eNMPC$_4$. During the control system design, the individual components of $x_p$ and $z$ are normalized through division by their maximum expected value.

### C. 5-D Problem (a): Internal Model

The model of Section III-B considers instantaneous generation of the longitudinal tire force. In this section, the model is enhanced to account for the tire force dynamics, by including the concept of tire relaxation length, $\sigma$. A first-order differential equation calculates the slip ratio for the MF in (26) and (28), starting from the wheel speed and vehicle speed. By assuming a linear dependency between the longitudinal tire force and vertical load the first-order longitudinal tire force dynamics are implemented. The resulting internal model is described by the differential equations (29)–(32):

$$\frac{d}{dt}s(t) = \left(-\frac{r^2}{J_w} - \frac{1}{m}\right)D\sin\left(C\arctan\left(B\sigma_x^{rel}(t)\right)\right)F_z + \frac{(T_{CA} - \Delta T(t))r}{J_w} \tag{29}$$

$$\frac{d}{dt}e_{int}(t) = s(t) - \sigma_x^{ref}\omega(t)r \tag{30}$$

$$\frac{d}{dt}\omega(t) = \frac{1}{J_w}\left(T_{CA} - \Delta T(t) - D\sin\left(C\arctan\left(B\sigma_x^{rel}(t)\right)\right)F_z r\right) \tag{31}$$

$$\frac{d}{dt}\sigma_x^{rel}(t) = \frac{(\omega(t)r - s(t))}{\sigma}\left(\frac{s(t)}{\omega(t)r} - \sigma_x^{rel}(t)\right). \tag{32}$$

In this case, the state vector, input vector, and parameter vector are, respectively, $x = [s, e_{int}, \omega, \sigma_x^{rel}]$, $u = [\Delta T]$, and $p = [T_{CA}]$. The problem includes five parameters (5-D problem), i.e., $x_p = [s(t_k), e_{int}(t_k), \omega(t_k), \sigma_x^{rel}(t_k), T_{CA}(t_k)]$, and five decision variables, i.e., $z = [\Delta T(t_k), \Delta T(t_{k+1}), \Delta T(t_{k+2}), \Delta T(t_{k+3}), \nu(t_k)]$. The respective explicit controller will be called eNMPC$_{5a}$ in the remainder.

### D. 5-D Problem (b): Internal Model

The model of Section III-B considers a constant value of the vertical tire load. In this section, a more accurate case is considered, where the vertical tire load is computed as a function of the vehicle longitudinal and lateral accelerations. The estimated vertical load value becomes a slowly varying parameter for the control problem, thus increasing its dimension.

In this case, the equations of the system are exactly the same as in Section III-B, but the state vector, input vector, and parameter vector are, respectively, $x = [s, e_{int}, \omega]$, $u = [\Delta T]$ and $p = [T_{CA}, F_z]$. The problem now includes five parameters (5-D problem), i.e., $x_p = [s(t_k), e_{int}(t_k), \omega(t_k), T_{CA}(t_k), F_z(t_k)]$, and five decision variables, i.e., $z = [\Delta T(t_k), \Delta T(t_{k+1}), \Delta T(t_{k+2}), \Delta T(t_{k+3}), \nu(t_k)]$. The respective implicit controller will be called NMPC$_{5b}$ in the remainder.

### E. Control Problem Formulation

The three internal models of Sections III-B–III-D share the same optimal control problem formulation. The continuous

form of the cost function is

$$V = \int_{t_k}^{t_f} \frac{q_{x1}}{w_{x1}^2}(s(t) - \sigma_x^{\text{ref}}\omega(t)r)^2 + \frac{q_{x2}}{w_{x2}^2}e_{\text{int}}(t)^2$$
$$+ \frac{r_u}{w_u^2}\Delta T(t)^2 + \frac{r_v}{w_v^2}v(t_k)^2 dt + \frac{p_{x1}}{w_{x1}^2}(s(t_f)$$
$$- \sigma_x^{\text{ref}}\omega(t_f)r)^2 + \frac{p_{x2}}{w_{x2}^2}e_{\text{int}}(t_f)^2 \tag{33}$$

where $q_{x1}$, $q_{x2}$, $r_u$, $r_v$, $p_{x1}$, and $p_{x2}$ are the weights for the different terms, and the notations $w_i$ indicate scaling factors. As a consequence, a tracking problem is set for the first state $s$ and a regulating problem is set for the second state, $e_{\text{int}}$.

The choice of adopting the slip velocity $s$ as state and tracking variable, rather than the more commonly used slip ratio $\sigma_x$, finds its motivation in the algorithm for the computation of the explicit solution. In fact, the adoption of $\sigma_x$ would lead to a feedback law that is scaled with the angular wheel speed. The higher variability of the feedback control law would imply a finer partition of the space, to reach a good approximation of the nonlinear problem. Hence, the choice of different internal models, although equivalent from the viewpoint of the represented physics, influences the efficiency of the generation of the explicit solution. Careful consideration of this aspect in the design phase leads to a reduction of the off-line computational burden and the on-line memory requirement.

The minimization of (33) is subject to state and input bound constraints

$$s_{\min} - v \leq s \leq s_{\max} + v \tag{34}$$
$$0 \leq \Delta T \leq T_{\text{CA}}. \tag{35}$$

## IV. ENMPC-BASED TC IMPLEMENTATION

An advantage of eNMPC with respect to implicit NMPC is the availability of the feedback control law beforehand. This allows the analysis of the control action for any value of the vector of parameters.

The solution of the eNMPC$_4$, i.e., the 4-D eNMPC (see Section III-B), is presented in Fig. 2. To plot the 3-D surface in Fig. 2, two parameters have been fixed, i.e., the normalized integral of the wheel slip error, $x_p(2)$, which is set to zero, and the normalized wheel angular velocity, $x_p(3)$, which is set to 0.85. The red line "reference" indicates the wheel slip velocity corresponding to the reference slip ratio for the specific $x_p(3)$. $x_p(4)$ is the normalized torque demand from the CA.

The solution essentially consists of three planes:
1) a plateau of zero control action for low values of slip velocity, indicated as "input lower constraint" in Fig. 2. According to (35), the TC torque correction must be positive;
2) an inclined plane, parallel to the $x_p(1)$-axis, indicated as "input upper constraint" in Fig. 2, which expresses that, according to (35), the regulating torque cannot be larger than the torque demand;
3) another inclined plane, i.e., the "non-saturated feedback law," which is saturated by the previous two.
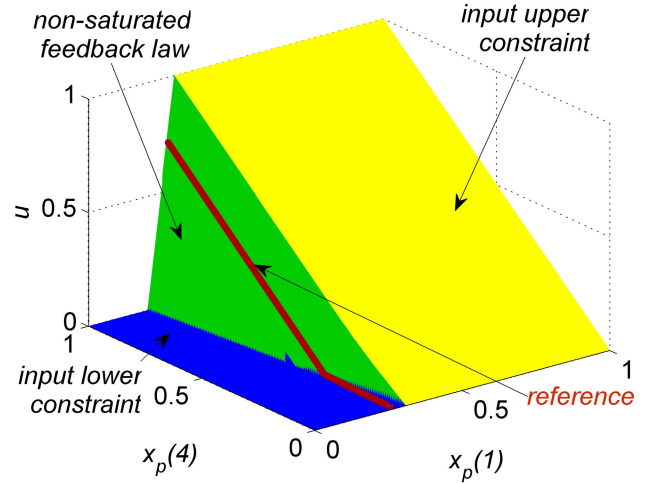


Fig. 2. Normalized control action $u$ for the 4-D problem as a function of $x_p(1)$ (normalized wheel slip velocity) and $x_p(4)$ (normalized torque demand from the driver).
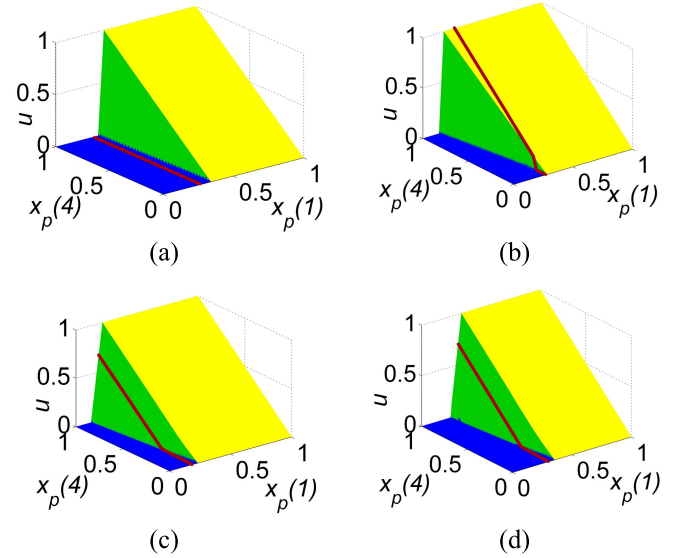


Fig. 3. Effect of $x_p(2)$ and $x_p(3)$ on $u$ for the 4-D problem. (a) Negative value of $x_p(2)$. (b) Positive value of $x_p(2)$. (c) Low value of $x_p(3)$. (d) High value of $x_p(3)$.

The analysis of the control action shows that no regulation is applied until the reference slip is reached, if the normalized torque demand is small. On the other hand, for high values of $x_p(4)$, a regulation is prescribed even before reaching the reference, based on the prediction available to the controller. Beyond the reference a regulation that is below the maximum possible value is applied for the whole range of torque demands, as long as the slip velocity is lower than a specific nonconstant value (see the surface "non-saturated feedback law"). Above this value the regulating control action is equal to the torque demand, i.e., $u = x_p(4)$.

The effect of the normalized integral of the slip velocity error, $x_p(2)$, is presented in Fig. 3(a) and (b), corresponding to a negative value and a positive value of $x_p(2)$, respectively. The whole surface of the feedback law shifts along the
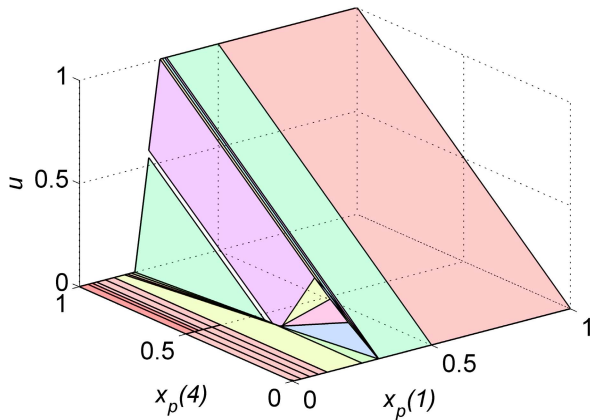
Fig. 4. Normalized control action with the corresponding region indication. $x_p(2)$ and $x_p(3)$ have been fixed.

$x_p(1)$-axis, while the reference does not move. This acts as a compensation for the initial positive or negative value of $x_p(2)$. Fig. 3(c) and (d) shows the variation of the feedback law with the normalized wheel speed, $x_p(3)$. Although the shape of the surface does not change, it translates with the reference slip velocity along the $x_p(1)$-axis. Fig. 4 shows that the piecewise affine feedback law is actually evaluated from a number of different regions of the parametric problem, i.e., hyper-rectangles and polyhedral critical regions, despite the control action mainly consists of only three planes. The analysis of Figs. 2–4 suggests that the whole feedback law could be realized as a ruled-based strategy that defines different planes intersections and translations, given the input measurements from the plant. Alternatively, a rigorous method for the reduction of the memory requirements of explicit model predictive controllers is presented in [34].

During the implementation phase of the eNMPC, as shown in Fig. 1, a specific strategy was applied for the compensation of $\delta_m$ and $\delta_{CAN}$, i.e., the pure time delays associated with the electric motor drive and the CAN bus, respectively. The adopted technique is based on the concept used in [16] for a hybrid explicit MPC implementation of a TC. A state predictor, employing the same model formulation described in Section III-B, and a buffer, containing part of the past control history, are used to predict the trajectory of the input parameters to the eNMPC, for a horizon length of $\delta_m + \delta_{CAN}$. Thus, the inputs to the controller are projected into the future, and the control action is computed based on this prediction.

The solution of the eNMPC$_4$ was tested on a dSPACE MicroAutobox II (900 MHz, 16 MB) rapid control prototyping unit. An exploration of the parameter space was performed to assess the computational time for a fine and comprehensive grid of possible inputs. The computational time for the combination of the two function evaluation layers was in the range of ∼5–25 $\mu$s. These values are very low compared to the implementation time step of 2 ms, which is not achievable with more conventional implicit NMPC technology on the same hardware. Hence, the eNMPC can run in real-time at any frequency within the range typical of TC applications.

| Description | Value | Unit |
|---|---|---|
| Vehicle mass | 450 | kg |
| Wheel + motor mass moment of inertia | 1.5 | kgm² |
| Wheelbase | 1.875 | m |
| Wheel radius | 0.279 | m |
| Maximum single motor torque | 500 | Nm |
| Motor time constant ($\tau_m$) | 0.5 | ms |
| Motor time delay ($\delta_m$) | 1 | ms |
| CAN bus time delay ($\delta_{CAN}$) | 3 | ms |

## V. SIMULATION RESULTS

### A. Test Scenario and Evaluation Metrics

The simulation analysis was carried out with a high fidelity vehicle simulation model implemented with the software IPG CarMaker. The vehicle data (see Table II) are those of an electric quadricycle prototype with a front-wheel-drive topology, based on two in-wheel motors (direct drive) with a peak torque of 500 Nm each. Given the low mass of the vehicle, the available torque is sufficient to provoke front wheel spinning even in high tire-road friction conditions.

The tire model is the MF (ver. 5.2), and includes the variation of the longitudinal and lateral relaxation lengths as functions of the vertical load. The electric motor dynamics are modeled through a first order transfer function and a pure time delay. A pure time delay is also considered on the controller output to model the CAN bus [32]. Unless otherwise specified, in the remainder the implementation time step of the controllers, $t_{S,I}$, is of 2 ms.

The considered acceleration test scenario is based on a straight road with varying tire-road friction coefficient, $\mu$. The values of $\mu$ are modified in steps, according to the sequence 0.9–0.15–0.9–0.45–0.9. This provides a real challenge to the TC, which has to regulate the slip ratio to a constant reference value of 0.10, while the vehicle is accelerating from an initial speed of 5 km/h, at which a fast torque demand ramp up to the drivetrain peak torque is imposed.

To objectively assess the TC performance, a set of performance indicators is identified based on [20].

1) The root-mean square value of the slip ratio error, i.e., a tracking performance indicator

$$\text{RMSE} = \sqrt{\frac{1}{t_e - t_i} \int_{t_i}^{t_e} (\sigma_x(t) - \sigma_x^{\text{ref}})^2 dt} \qquad (36)$$

where $\sigma_x(t)$ is the actual value of the slip ratio during the relevant part of the test, defined by the initial and final times $t_i$ and $t_e$.

2) The final value of vehicle velocity, $V_f$, i.e., an acceleration performance indicator.

3) The normalized integral of the absolute value of the control action, which gives an indication of the required control effort

$$\text{IACA} = \frac{1}{t_e - t_i} \int_{t_i}^{t_e} |\Delta T(t)| \, dt. \qquad (37)$$
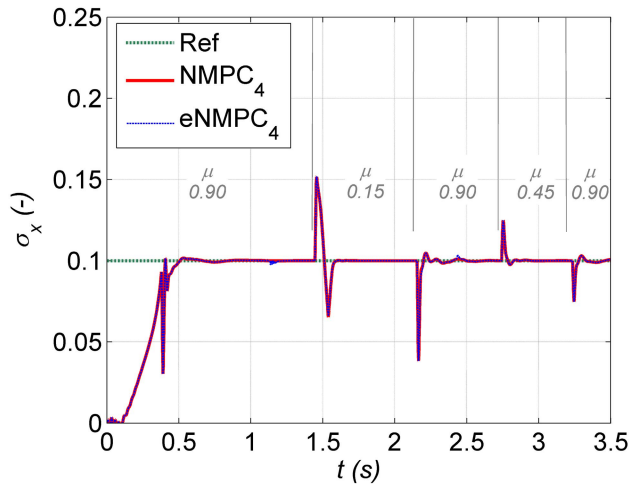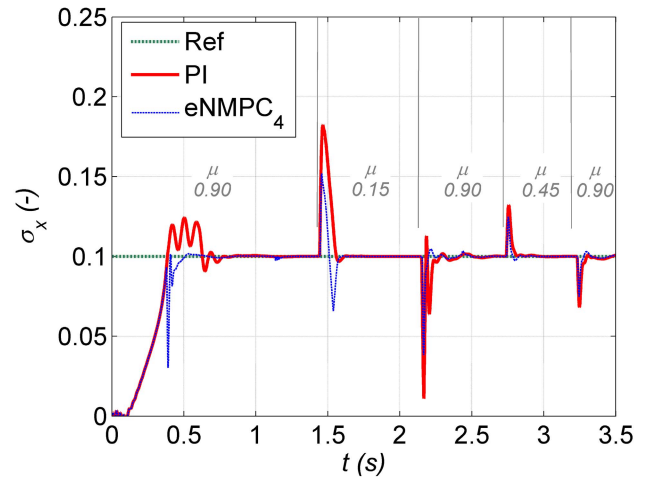
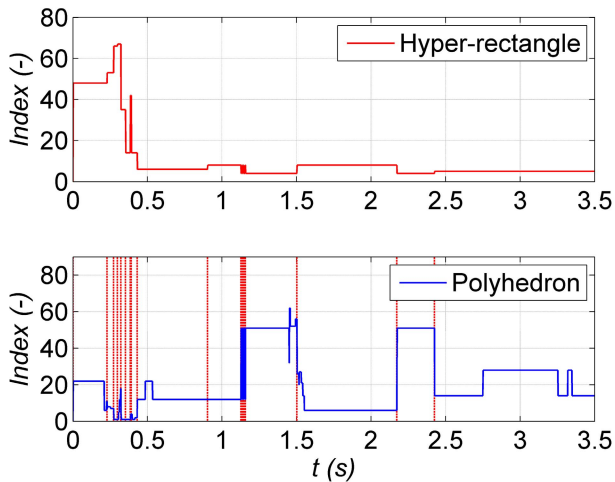Fig. 5.   NMPC$_4$ and eNMPC$_4$ comparison: actual and reference slip ratios of the front left wheel.



Fig. 6.   eNMPC$_4$: hyper-rectangle index (top) and polyhedral critical region index (bottom) with the vertical lines indicating the hyper-rectangle switching times. Each hyper-rectangle has an independent numbering of its polyhedra.

### B. eNMPC$_4$ Benchmarking

To prove the effectiveness of the local quadratic approximations of the multi-parametric nonlinear problem, the simulation results for the described scenario are reported in Fig. 5, with an overlap between the eNMPC$_4$ solution and the corresponding implicit one. The implicit strategy for the 4-D case (NMPC$_4$) is implemented by solving on-line the same nonlinear optimal control problem with the same solver, IPOPT, employed for the generation of the explicit solution. The implicit strategy, which is not real-time capable, represents the optimal solution, because of the absence of the local quadratic approximations. Fig. 5 shows that the solutions of the NMPC$_4$ and eNMPC$_4$ are indistinguishable. As this is confirmed by all the simulations that were performed during the study, the level of sub-optimality of the eNMPC$_4$ implementation is considered satisfactory.

Fig. 6 reports the index of the hyper-rectangles that are used by the eNMPC$_4$ in the considered scenario, and the index of the polyhedral critical regions that are employed within each hyper-rectangle. The figure reveals that only a few



Fig. 7.   PI and eNMPC$_4$ comparison: actual and reference slip ratios of the front left wheel.

regions are used in the simulated complex scenario. Moreover, the crossings of different hyper-rectangle boundaries, which imply discontinuities in the solution, do not bring any significant degradation of the explicit feedback control action.

### C. eNMPC$_4$ and Proportional Integral (PI) Controller

The results of the eNMPC$_4$ are compared with those obtained through a simple yet effective PI-based TC system, with gain scheduling on vehicle speed and including anti-windup features on its integral contribution.

A frequency response-based initial design of the PI gains was performed with a linearized plant model for different vehicle speeds. This was followed by an empirical fine tuning through simulations in the time domain with the CarMaker model. The gains obtained with this process were finally reassessed by employing the linearized plant to verify gain and phase margins, as well as the sensitivity and complementary sensitivity functions.

The comparison of the controller results in terms of slip ratios is reported in Fig. 7. For both the PI and the eNMPC$_4$ the TC is activated in proximity of the reference slip value, $\sigma_x^{ref}$. The response of the two controllers to the initial wheel torque demand application presents visible differences. The PI overshoots $\sigma_x^{ref}$, and then reaches the desired value with a damped oscillatory response. The eNMPC$_4$ presents an initial undershoot caused by the controller activation and the discrepancy between the tire-road friction coefficients of the plant and the internal model. This is promptly recovered by the integral action. Afterwards, the eNMPC$_4$ approaches the reference more gently, with a lower overshoot and less oscillations. The reason for this behavior is that the design of the eNMPC$_4$ TC is based on tire characteristics for $\mu = 0.45$. Hence, when the controller operates in higher tire-road friction conditions (e.g., at $\mu = 0.9$), it tends to be conservative. Nevertheless, $\sigma_x^{ref}$ is reached at approximately the same time as in the PI case. The transition between $\mu = 0.9$ and $\mu = 0.15$ is very demanding for the controllers. The PI responds with an overshoot that is maintained until the slip
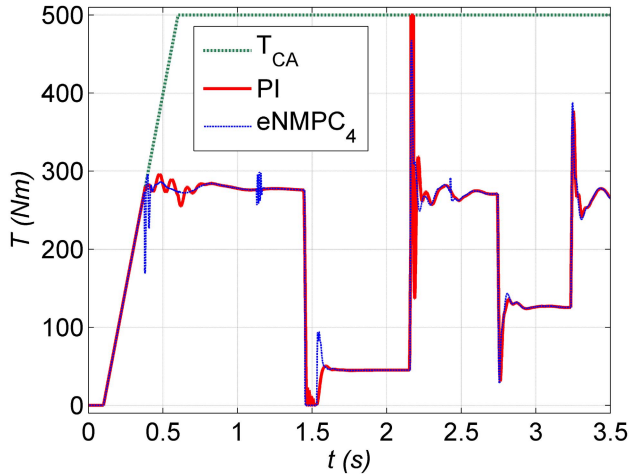
Fig. 8.   PI and eNMPC$_4$ comparison: torques before and after the front left TC block.
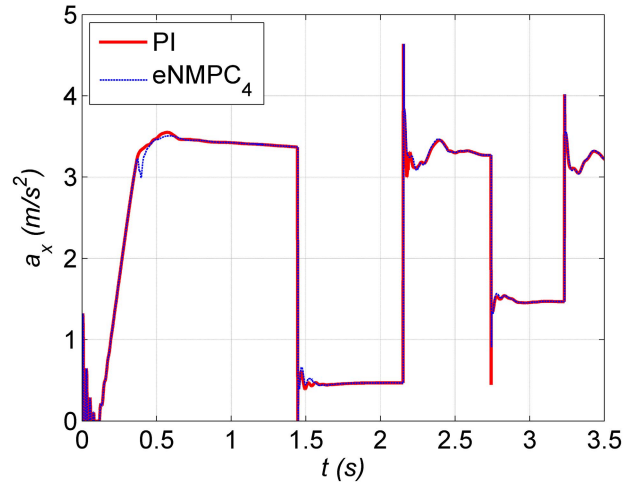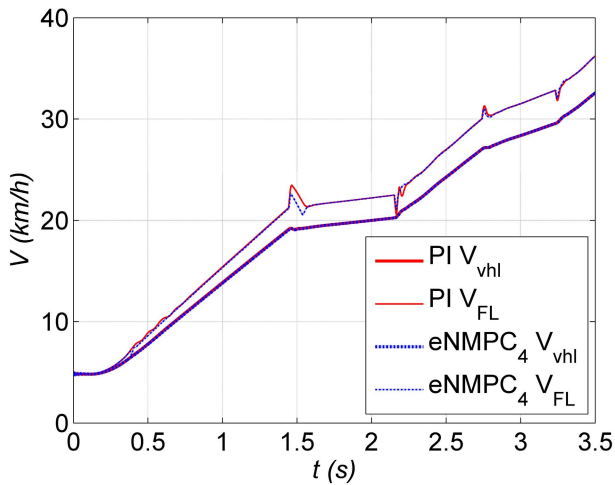


Fig. 9.   PI and eNMPC$_4$ comparison: front left wheel speed multiplied by the wheel radius, $V_{FL}$, and vehicle velocity, $V_{vhl}$.



Fig. 10.   PI and eNMPC$_4$ comparison: longitudinal acceleration of the vehicle.

TABLE III
SUMMARY OF PERFORMANCE INDICATORS AND RESPECTIVE VARIATIONS

| Case No. | Controller | $t_{S,I}$ (s) | RMSE (-) | $V_f$ (km/h) | IACA (Nm) |
|---|---|---|---|---|---|
| i | (a) PI | 0.002 | 0.02301 | 35.242 | 267.82 |
| iv | (b) eNMPC$_4$ | 0.002 | 0.02089 | 35.259 | 267.89 |
|  | Δ% w.r.t. (a) | - | - 9.2% | + 0.05% | + 0.03% |
| v | eNMPC$_4$* | 0.004 | 0.02301 | 35.242 | 268.28 |
|  | Δ% w.r.t. (b) | - | + 10.1% | - 0.05% | + 0.15% |
| vi | eNMPC$_4$*** | 0.004 | 0.02269 | 35.249 | 268.23 |
|  | Δ% w.r.t. (b) | - | + 8.6% | - 0.03% | + 0.08% |
| v | eNMPC$_4$* | 0.008 | 0.04855 | 34.960 | 272.49 |
|  | Δ% w.r.t. (b) | - | + 132.4% | - 0.85% | + 1.72% |
| vi | eNMPC$_4$*** | 0.008 | 0.03732 | 35.112 | 270.12 |
|  | Δ% w.r.t. (b) | - | + 78.6% | - 0.42% | + 0.83% |
| ii | PI ** | 0.004 | 0.02655 | 35.222 | 268.05 |
|  | Δ% w.r.t. (a) | - | + 15.4% | - 0.05% | + 0.08% |
| iii | PI *** | 0.004 | 0.02486 | 35.225 | 267.95 |
|  | Δ% w.r.t. (a) | - | + 8.0% | - 0.05% | + 0.05% |
| ii | PI ** | 0.008 | 0.06558 | 34.150 | 274.30 |
|  | Δ% w.r.t. (a) | - | + 185.1% | - 3.10% | + 2.42% |
| iii | PI *** | 0.008 | 0.03719 | 35.090 | 269.19 |
|  | Δ% w.r.t. (a) | - | + 61.7% | - 0.43% | + 0.51% |

 \*    no re-tuning
 \*\*   anti-wind-up gain retuning (otherwise unstable)
 \*\*\*  full retuning

ratio reaches $\sigma_x^{\text{ref}}$. For the eNMPC$_4$ the overshoot presents a smaller peak and a faster response leading to the reference. This is followed by a promptly recovered undershoot. The next difficult transition is the one that leads back to $\mu = 0.9$. In this case, both controllers present undershoots followed by a few oscillations with similar duration. The oscillations have higher amplitudes for the PI. In the final $\mu$-transitions the overshoots and undershoots are relatively small and of similar magnitude for the two controllers, although slightly higher for the PI, which also exhibits a slower response.

Fig. 8 shows the wheel torques before and after the TC block. Similarly to the slip ratios, the time histories highlight the marginally faster response of the eNMPC$_4$, together with the more quickly damped oscillations of its control action. Fig. 9 shows the angular speed of the front left wheel, multiplied by the wheel rolling radius, and the vehicle speed. The time histories of the longitudinal vehicle acceleration are reported in Fig. 10. The wide range of values, i.e., from ∼0 to ∼4.5 m/s² during the relevant part of the test, together with their abrupt variations, confirms the high level of

severity of the selected scenario. The longitudinal acceleration does not significantly differ among the two controllers.

Table III reports the objective performance indicators defined in Section V-A for Cases i–vi.

*Case i:* The PI TC running at $t_{S,I} = 2$ ms. During the implementation phase of the controller it was verified that a further reduction of $t_{S,I}$ within reasonable limits would not have brought substantial benefits.

*Case ii:* The PI TC running at 4 and 8 ms, with the same gains as for Case i, apart from the anti-windup gain. The variation of the anti-windup gain was necessary to provide control system stability in the selected test, especially immediately after the first $\mu$-transition.

*Case iii:* The PI TC running at 4 and 8 ms with optimized gains for those time steps. The PI gain optimization was based on CarMaker simulations of the selected

maneuver, and was aimed at the minimization of the slip ratio RMSE.

*Case iv:* The eNMPC$_4$ TC running at 2 ms.

*Case v:* The eNMPC$_4$ TC running at 4 and 8 ms, with the same weights of the cost function, the same discretization interval $t_s$ of the internal model and the same prediction horizon $t_p$ as for Case iv. In the 4-ms subcase, in the eNMPC$_4$ off-line process it is imposed $\Delta T(t_k) = \Delta T(t_{k+1})$ and $\Delta T(t_{k+2}) = \Delta T(t_{k+3})$, while in the 8-ms subcase it is imposed $\Delta T(t_k) = \Delta T(t_{k+1}) = \Delta T(t_{k+2}) = \Delta T(t_{k+3})$.

*Case vi:* The eNMPC$_4$ TC running at 4 and 8 ms, with a fine-tuning of the weights of its cost function. Similarly to Case iii, the eNMPC$_4$ tuning process consisted of CarMaker model simulations and iterative computations of the slip ratio RMSE.

The comparison between Case i and Case iv shows a 9.2% reduction of the RMSE for the eNMPC$_4$ TC compared to the PI TC, together with a negligible increment on the final velocity and IACA. Both the PI TC and eNMPC$_4$ TC are subject to a significant decay of the respective tracking performance, when they are implemented at 4 and 8 ms without modifying their design with respect to the cases running at 2 ms. In particular, the RMSE increase is of 15.4% and 185.1% for the PI controller, while it is of 10.1% and 132.4% for the eNMPC$_4$. If the PI TC and eNMPC$_4$ TC are retuned for the time steps of 4 and 8 ms, the performance decay is still significant, i.e., it amounts to 8% and 61.7% for the PI, and 8.6% and 78.6% for the eNMPC$_4$. It is possible to observe the following.

1) For the specific application significant retuning of the controller is needed when changing the time step, which is an important outcome, not reported in the existing TC literature to the knowledge of the authors; and

2) The performance decay induced by the increase of $t_{S,I}$ is relatively similar for the two control structures.

These results can be justified through the analysis of the linearized model of the plant without TC, including consideration of tire relaxation. The linearization was carried out in proximity of the reference slip ratio. At a vehicle speed of 2.5 m/s the slip ratio response to a motor torque step input has a rise time, $T_r$, of only ∼5 ms, which becomes ∼11 and ∼26 ms, respectively, at 5 and 10 m/s. The very fast response is related to the in-wheel layout of the specific electric drivetrains. Based on the indications in [35], the implementation time step should range from 6% to 40% of $T_r$. For the average speed of the simulated scenario, i.e., ∼5 m/s, this implies a recommended range of $t_{S,I}$ from 0.7 to 4.4 ms. At the initial speed of the simulated tests the recommended time step would be even significantly lower. Therefore, the system rise time values are consistent with the TC performance degradation for $t_{S,I} = 4$ ms and $t_{S,I} = 8$ ms, where the latter is nearly twice the maximum recommended time step at 5 m/s.

In summary, a low value of the implementation time step at which the TC is run guarantees a significant enhancement of the results, independently of the selected controller. It should be noted that in many practical TC applications the time step
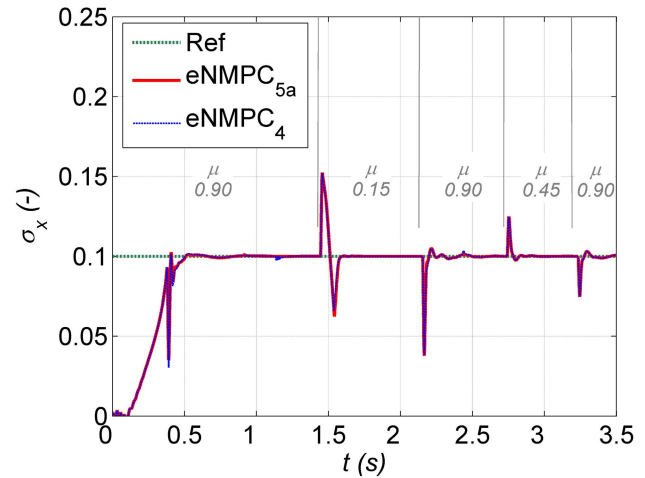


Fig. 11. eNMPC$_4$ and eNMPC$_{5a}$ comparison: reference and actual slip ratios.

is of ∼10 ms. In particular, the eNMPC$_4$ TCs at 4 and 8 ms, respectively, provide similar and worse results than the PI TC at 2 ms, which means that the appropriate selection of $t_{S,I}$ should have higher priority in the TC design process with respect to the control structure selection, at least for electric vehicles with very responsive in-wheel motors such as that of this paper. Nonlinear MPC technology can be used to enhance the TC performance, but, this is actually beneficial only if the NMPC is run at 2 ms. In such a condition the NMPC provides better results than the PI controller, that can be easily implemented with a very low time step. However, with the available computing hardware for automotive applications, an implicit NMPC does not currently run at 2 ms, and possibly not even safely at 4 ms, according to the literature mentioned in Section I. This makes the implementation of the eNMPC$_4$, rather than an implicit NMPC$_4$, necessary and beneficial to achieve the potential vehicle performance benefits.

### D. Effect of Tire Force Dynamics Modeling

This section evaluates the effect of considering the longitudinal tire force dynamics in the internal model for NMPC design. The simulation results for the eNMPC$_{5a}$ TC, derived from the internal model of Section III-C, are reported in Fig. 11 for the considered $\mu$-varying scenario. The addition of the relaxation length does not bring any benefit in terms of tracking performance. The reason is related to the relative fast dynamics of the longitudinal tire force generation, especially, for higher vehicle velocities and a flat road surface. The eNMPC$_{5a}$ implementation shows that a 5-D problem can also be managed with this control methodology.

### E. Effect of Time-Varying Vertical Load Modeling

This section studies the effect of including the variable vertical tire load in the internal model of the NMPC (see Section III-D). Since it has been proven that the generated explicit solution for the eNMPC$_4$ shows no visible difference from its corresponding implicit solution, i.e., the NMPC$_4$, the comparison for this particular internal modeling feature will be carried out only through the implicit strategy.
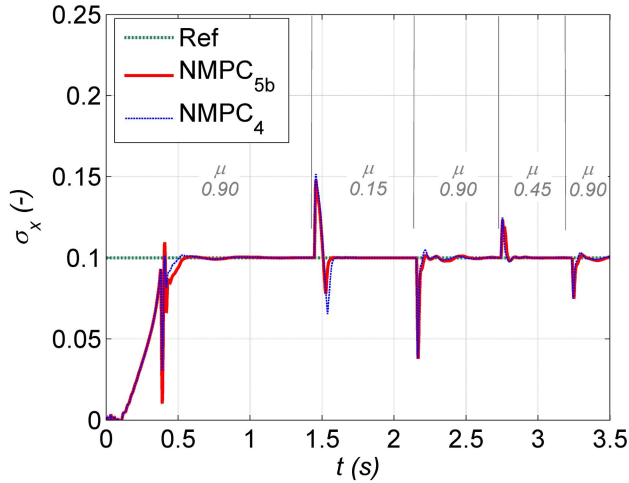
Fig. 12. NMPC$_4$ and NMPC$_{5b}$ comparison: actual and reference slip ratios of the front left wheel.

Fig. 12 shows the results of this comparison along the simulated scenario. The performance of the two controllers is very similar. In the first part of the scenario, when $\mu = 0.9$, the NMPC$_4$ shows a slightly better response. In the rest of the test the NMPC$_{5b}$ provides better tracking. Overall, the difference is very limited, and it amounts to less than 0.5% in terms of RMSE. It can be concluded that, in this application, to increase the dimension of the problem by introducing a time-varying vertical load does not provide any major benefit with respect to the 4-D problem with constant load.

Future research will focus on the evaluation of alternative selections of the fifth parameter of the controller. For example, additional parameters could include a time-varying $\sigma_x^{\text{ref}}$, to improve the lateral tire force capability, as shown in [36], or to provide better performance when starting from standstill.

### F. Robustness Assessment

The robustness against the variation of the tire-road friction coefficient $\mu$ has already been assessed. In this section, further simulations are performed with the eNMPC$_4$ and the PI, with $t_{S,I} = 2$ ms.

Three vehicle parameters have been identified to have a potentially relevant effect on control system performance, namely: 1) the total vehicle mass, $M$; 2) the wheel mass moment of inertia, $J$; and 3) the longitudinal slip stiffness of the tires, $K_x$. The results in terms of RMSE and corresponding percentage variation with respect to the baseline condition of the controllers are reported in Table IV.

For a $+/-15\%$ variation of $M$, the results show that the RMSE increase/decrease for the eNMPC$_4$ (Cases vii and viii) is confined to $+5.1\%$ and $-5.4\%$. The same applies to cases ix and x, i.e., to the PI TC, with $+6.1\%$ and $-5.6\%$. Hence, the addition of a passenger or payload does not significantly affect the TC tracking performance. When a $+/-30\%$ variation of $J$ is imposed, the eNMPC$_4$ (Cases xi and xii) and the PI (Cases xiii and xiv) present the same very marginal performance degradation (i.e., by 0.4% and 2.5%). This means that the controllers will be effec-

#### TABLE IV
#### ROBUSTNESS ASSESSMENT: VEHICLE PARAMETERS VARIATION EFFECT ON TRACKING PERFORMANCE

| Case No. | Controller | Vehicle parameter change | RMSE (-) |
|---|---|---|---|
| i | (a) PI | - | 0.02301 |
| iv | (b) eNMPC$_4$ | - | 0.02089 |
| vii | eNMPC$_4$* | $M + 15\%$ | 0.02195 |
| | Δ% w.r.t. (b) | - | + 5.1% |
| viii | eNMPC$_4$* | $M - 15\%$ | 0.01977 |
| | Δ% w.r.t. (b) | - | - 5.4% |
| xi | eNMPC$_4$* | $J + 30\%$ | 0.02097 |
| | Δ% w.r.t. (b) | - | + 0.4% |
| xii | eNMPC$_4$* | $J - 30\%$ | 0.02141 |
| | Δ% w.r.t. (b) | - | + 2.5% |
| xv | eNMPC$_4$* | $K_x + 20\%$ | 0.02187 |
| | Δ% w.r.t. (b) | - | + 4.7% |
| xvi | eNMPC$_4$* | $K_x - 20\%$ | 0.01959 |
| | Δ% w.r.t. (b) | - | - 6.2% |
| ix | PI* | $M + 15\%$ | 0.02440 |
| | Δ% w.r.t. (a) | - | + 6.1% |
| x | PI* | $M - 15\%$ | 0.02173 |
| | Δ% w.r.t. (a) | - | - 5.6% |
| xiii | PI* | $J + 30\%$ | 0.02311 |
| | Δ% w.r.t. (a) | - | + 0.4% |
| xiv | PI* | $J - 30\%$ | 0.02359 |
| | Δ% w.r.t. (a) | - | + 2.5% |
| xvii | PI* | $K_x + 20\%$ | 0.02421 |
| | Δ% w.r.t. (a) | - | + 5.2% |
| xviii | PI* | $K_x - 20\%$ | 0.02173 |
| | Δ% w.r.t. (a) | - | - 5.6% |

\* no re-tuning

#### TABLE V
#### ROBUSTNESS ASSESSMENT: NOISE INJECTION EFFECT ON TRACKING PERFORMANCE

| Case No. | Controller | Test condition | RMSE (-) | Maximum $\sigma_x$ |
|---|---|---|---|---|
| i | (a) PI | - | 0.02301 | 0.182 |
| iv | (b) eNMPC$_4$ | - | 0.02089 | 0.152 |
| xix | eNMPC$_4$* | noise on $\omega_i$ with $i = FL, FR, RL, RR$ | 0.05065 | 0.195 |
| | Δ% w.r.t. (b) | - | + 142.5% | + 28.3% |
| xx | PI* | noise on $\omega_i$ with $i = FL, FR, RL, RR$ | 0.08984 | 0.350 |
| | Δ% w.r.t. (a) | - | + 290.5% | + 92.3% |

\* no re-tuning

tive for a wide range of wheel characteristics. Finally, also when $K_x$ is varied by $+/-20\%$ to consider different tire properties, the RMSE variation is limited, and it amounts to $+4.7\%$ and $-6.2\%$ for Cases xv and xvi (eNMPC$_4$), and to $+5.2\%$ and $-5.6\%$ for Cases xvii and xviii (PI). In conclusion, both controllers are robust for the considered reasonable range of plant parameter variations, with a limited advantage of the eNMPC$_4$ over the PI.

Another aspect of control system robustness is the noise rejection performance. The sensor noise resulting from a real vehicle prototype test, presented later on in this paper, was analyzed. Gaussian white noise with different initial seeds is added to the simulated wheel speeds of each corner. These are the main input signals of the controller, which are used to compute the slip ratio. The results are reported in Table V, in terms of RMSE variation and maximum slip ratio throughout the scenario. The comparison is made with respect to the same controllers without the noise injection.

Fig. 13. Electric vehicle prototype during the TC and passive vehicle experimental test session on the low-$\mu$ metal plates. The vehicle skids laterally when the TC is deactivated (bottom).

In the Case xix, the eNMPC$_4$ is still able to follow the reference throughout different $\mu$ variations. The RMSE increase is of 142.5%, and is mainly caused by oscillations around the reference. The peak values of slip ratio remain similar to the case without noise injection, with a maximum increase of 28.3%. The PI presents a very different situation. The controller is no longer able to follow the reference closely in all friction conditions. This is evident from the 290.5% RMSE increase, and the 92.3% increase of the maximum value of $\sigma_x$. Although the PI controller is still able to eventually recover the tracking of the reference slip ratio, the eNMPC$_4$ presents much better noise rejection characteristics. It must be noted that these results were obtained without retuning of the controllers. This operation is recommended for obtaining desirable performance in case of noisy signals.

## VI. EXPERIMENTAL RESULTS

An experimental testing session was conducted with the eNMPC$_4$ TC on the electric quadricycle prototype of the European H2020 SilverStream project. The vehicle has a mass of 640 kg (driver excluded), and is equipped with four in-wheel motors with a peak power of 4.2 kW and a peak torque of 115 Nm each. The prototype is shown in Fig. 13.

The tests were conducted in front-wheel-drive mode, on a series of smooth steel plates, which were lubricated to further decrease the friction coefficient. This is estimated to be $\sim$0.09–0.10. Similarly to the simulation scenarios, the vehicle was driven on the metal plates at speeds of 5–7 km/h and, then, the driver suddenly pressed the accelerator pedal to demand the maximum available torque from the front in-wheel motors. The pedal position was maintained until the end of the metal surface was reached. The eNMPC$_4$ with $t_{S,I} = 4$ ms was updated in terms of internal model parameters and input
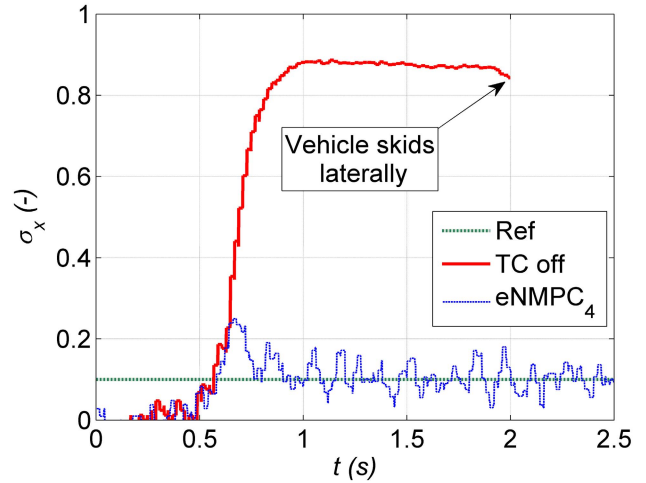


Fig. 14. Experimental tests: comparison of actual and reference slip ratios for the vehicle with the eNMPC$_4$ and the passive vehicle (TC off).
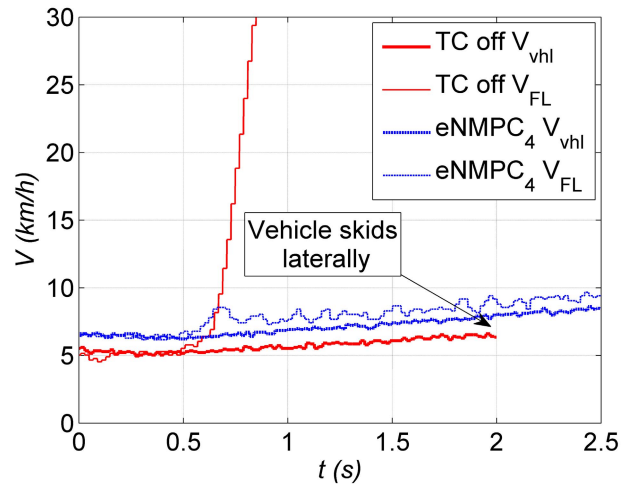


Fig. 15. Experimental tests: comparison of vehicle speed ($V_{vhl}$) and front left angular wheel speed multiplied by the wheel radius ($V_{FL}$) for the vehicle with the eNMPC$_4$ and the passive vehicle (TC off).

constraints, to take into account the greater vehicle mass and lower motor torque capability, with respect to the simulated scenarios.

The slip ratio time histories for the vehicle with the eNMPC$_4$ and the passive vehicle, i.e., the vehicle with deactivated TC, are presented in Fig. 14. In the passive vehicle $\sigma_x$ reaches values of almost 0.9. This affects the duration of the maneuver, since the lateral force capability of the front tires is drastically reduced, because of the coupling effect between longitudinal and lateral tire forces. Hence, the driver was not able to drive the vehicle in a straight line. For the eNMPC$_4$, after a first peak of 0.25, $\sigma_x$ goes back to the reference value of 0.10 in the following 0.2 s. The good tracking performance continues for the duration of the test with limited oscillations around the reference. Faster response and closer tracking were obtained with a different eNMPC$_4$ tuning, at the expense of increased motor torque oscillations.

Fig. 15 confirms the criticality of the friction conditions, with the front left tire of the passive vehicle that spins up
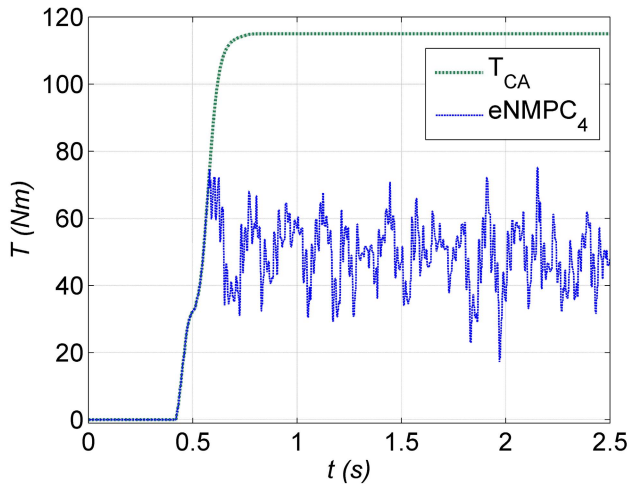
Fig. 16. Experimental tests: comparison of motor torque demand before ($T_{CA}$) and after the front left TC block for the vehicle with the eNMPC$_4$.

compared to the rear wheels, which provide the estimated vehicle speed. The vehicle velocity profiles with and without TC present similar trends. In fact, regardless of the considered road surface, when the slip ratio moves beyond the peak of longitudinal tire force, the $F_x$ reduction is limited and the vehicle acceleration is not substantially affected. In these conditions, the most important effect is the loss of lateral tire force capability, caused by the tire force coupling effect [37], which makes the passive vehicle skid laterally, and go outside the metal stripes [see Fig. 13 (bottom)].

Fig. 16 shows the electric motor torque regulation, with respect to the torque demand from the driver. The reduced torque settles at a value of ∼50 Nm, compared to the driver demand of 115 Nm, resulting in a ∼56% torque reduction. The torque oscillations, also caused by the nonconstant tire friction properties along the metal stripes, are reasonable for the specific implementation and the extreme testing conditions. Lower peak-to-peak oscillatory responses were obtained for higher tire-road friction levels during the experimental testing session.

## VII. Conclusion

This paper presented traction controllers for electric vehicles with in-wheel motors, based on explicit nonlinear model predictive control of the wheel slip velocity. These were compared with more conventional TC strategies based on PI control. The novel conclusions are as follows.

1) The implementation time step of the TC has a more significant impact on the control system performance than the selection of the control system technology. Employing nonlinear MPC is not enough to provide better performance than that of a PI running at an appropriate time step. To achieve a performance enhancement, for the case study TC application, time steps of ∼2 ms are recommended, rather than of 4 or 8 ms. Both for the PI TC and nonlinear MPC TC, the control system parameters have to be fine-tuned through tests in the time domain for the selected time step.

2) The presented explicit nonlinear MPC implementations are characterized by on-line computational times in the range of 5–25 $\mu$s on the adopted dSPACE MicroAutoBox rapid control prototyping unit. This means that the strategies could be potentially implemented at any reasonable frequency for automotive TC applications. On the contrary, based on the literature it would not be possible to run an equivalent implicit NMPC at the required time step of 2 ms.

3) The nonlinear model predictive controller allows a 9.2% tracking performance improvement with respect to a PI controller during the variable tire-road friction scenario, simulated with a high fidelity vehicle model.

4) The local multi-parametric quadratic approximation of the nonlinear problem, for the selected explicit nonlinear model predictive control method, does not bring perceivable performance differences with respect to the corresponding implicit nonlinear model predictive controller.

5) The consideration of tire force dynamics and vertical load transfers in the internal model for MPC system design has negligible effects on the TC performance during the simulated scenario.

6) The interpretation of the explicit nonlinear model predictive control law provides useful information on the effect of different input parameters on the control action. The piecewise affine control law can be approximated with only three planes.

7) An explicit nonlinear model predictive control strategy for TC has been successfully implemented on a fully electric prototype vehicle and presented in the literature for the first time, to the best of the authors' knowledge.

Future developments of the research will evaluate as follows.

1) The increase of the number of parameters of the explicit nonlinear model predictive control problem, and the implications in terms of memory requirements and performance benefits.

2) The possibility of simpler strategies able to replicate a similar control pattern with reduced memory requirements for the on-line implementation of the controller.

## References

[1] H. Fujimoto, J. Amada, and K. Maeda, "Review of traction and braking control for electric vehicle," in *Proc. IEEE Vehicle Power Propuls. Conf.*, Oct. 2012, pp. 1292–1299.

[2] S. Murata, "Innovation by in-wheel-motor drive unit," *Vehicle Syst. Dyn.*, vol. 50, no. 6, pp. 807–830, 2012.

[3] V. Ivanov, D. Savitski, K. Augsburg, and P. Barber, "Electric vehicles with individually controlled on-board motors: Revisiting the ABS design," in *Proc. IEEE Int. Conf. Mechatronics (ICM)*, Mar. 2015, pp. 323–328.

[4] M. Amodeo, A. Ferrara, R. Terzaghi, and C. Vecchio, "Wheel slip control via second-order sliding-mode generation," *IEEE Trans. Intell. Transp. Syst.*, vol. 11, no. 1, pp. 122–131, Mar. 2010.

[5] D. Yin, S. Oh, and Y. Hori, "A novel traction control for EV based on maximum transmissible torque estimation," *IEEE Trans. Ind. Electron.*, vol. 56, no. 6, pp. 2086–2094, Jun. 2009.

[6] T. A. Johansen, I. Petersen, J. Kalkkuhl, and J. Ludemann, "Gain-scheduled wheel slip control in automotive brake systems," *IEEE Trans. Control Syst. Technol.*, vol. 11, no. 6, pp. 799–811, Nov. 2003.

[7] M. Boisvert, P. Micheau, and J. Nadeau, "Nonlinear LQG slip controller based on an empirical model for a three wheel hybrid vehicle," in *Proc. IEEE Veh. Power Propuls. Conf. (VPPC)*, 2014, pp. 1–5.

[8] S. Anwar and B. Ashrafi, "A predictive control algorithm for an anti-lock braking system," SAE Tech. Paper 2002-01-0302, 2002.

[9] S. Anwar, "Brake-based vehicle traction control via generalized predictive algorithm," SAE Tech. Paper 2003-01-0323, 2003.

[10] R. de Castro, R. E. Araujo, M. Tanelli, S. Savaresi, and D. Freitas, "Torque blending and wheel slip control in EVs with in-wheel motors," *Vehicle Syst. Dyn., Int. J. Vehicle Mech. Mobility*, vol. 50, no. 1, pp. 71–94, Jul. 2012.

[11] C. Satzger, R. de Castro, A. Knoblach, and J. Brembeck, "Design and validation of an MPC-based torque blending and wheel slip control strategy," in *Proc. IEEE Intell. Veh. Symp.*, Jun. 2016, pp. 514–520.

[12] C. Satzger and R. de Castro, "Combined wheel-slip control and torque blending using MPC," in *Proc. Int. Conf. Connected Veh. Expo (ICCVE)*, Nov. 2014, pp. 618–624.

[13] C. Satzger and R. de Castro, "Predictive brake control for electric vehicles," *IEEE Trans. Veh. Technol.*, vol. 67, no. 2, pp. 977–990, Feb. 2018.

[14] D. Yoo and L. Wang, "Model based wheel slip control via constrained optimal algorithm," in *Proc. Int. Conf. Control Appl.*, Oct. 2007, pp. 1239–1246.

[15] L. Yuan, H. Zhao, H. Chen, and B. Ren, "Nonlinear MPC-based slip control for electric vehicles with vehicle safety constraints," *Mechatronics*, vol. 38, pp. 1–15, Sep. 2016.

[16] F. Borrelli, A. Bemporad, M. Fodor, and D. Hrovat, "An MPC/hybrid system approach to traction control," *IEEE Trans. Control Syst. Technol.*, vol. 14, no. 3, pp. 541–552, May 2006.

[17] M. S. Basrah, E. Siampis, E. Velenis, D. Cao, and S. Longo, "Wheel slip control with torque blending using linear and nonlinear model predictive control," *Vehicle Syst. Dyn.*, vol. 55, no. 11, pp. 1665–1685, 2017.

[18] F. Bottiglione, A. Sorniotti, and L. Shead, "The effect of half-shaft torsion dynamics on the performance of a traction control system for electric vehicles," *Proc. Inst. Mech. Eng. D, J. Automobile Eng.*, vol. 226, no. 9, pp. 1145–1159, 2012.

[19] V. Ivanov, D. Savitski, and B. Shyrokau, "A survey of traction control and antilock braking systems of full electric vehicles with individually controlled electric motors," *IEEE Trans. Veh. Technol.*, vol. 64, no. 9, pp. 3878–3896, Sep. 2014.

[20] S. De Pinto, C. Chatzikomis, A. Sorniotti, and G. Mantriota, "Comparison of traction controllers for electric vehicles with on-board drivetrains," *IEEE Trans. Veh. Technol.*, vol. 66, no. 8, pp. 6715–6727, Aug. 2017.

[21] J. A. Grancharova and T. A. Johansen, *Explicit Nonlinear Model Predictive Control: Theory and Applications*, vol. 429. Berlin, Germany: Springer, 2012.

[22] T. A. Johansen, "On multi-parametric nonlinear programming and explicit nonlinear model predictive control," in *Proc. 41st IEEE Conf. Decis. Control.*, vol. 3, Dec. 2002, pp. 2768–2773.

[23] L. F. Domínguez and E. N. Pistikopoulos, "Recent advances in explicit multiparametric nonlinear model predictive control," *Ind. Eng. Chem. Res.*, vol. 50, no. 2, pp. 609–619, 2011.

[24] P. Tøndel and T. A. Johansen, "Lateral vehicle stabilization using constrained nonlinear control," in *Proc. Eur. Control Conf.*, no. 1, Sep. 2003, pp. 1887–1892.

[25] M. Herceg, M. Kvasnica, C. N. Jones, and M. Morari, "Multi-parametric toolbox 3.0," in *Proc. Eur. Control Conf.*, 2013, pp. 502–510.

[26] A. Wächter and L. T. Biegler, "On the implementation of a primal-dual interior point filter line search algorithm for large-scale nonlinear programming," *Math. Program.*, vol. 106, no. 1, pp. 25–57, Mar. 2006.

[27] H. Chen and F. Allgöwer, "A quasi-infinite horizon nonlinear model predictive control scheme with guaranteed stability," *Automatica*, vol. 34, no. 10, pp. 1205–1217, 1998.

[28] D. Q. Mayne, J. B. Rawlings, C. V. Rao, and P. O. M. Scokaert, "Constrained model predictive control: Stability and optimality," *Automatica*, vol. 36, no. 6, pp. 789–814, 2000.

[29] L. Grüne, "Analysis and design of unconstrained nonlinear MPC schemes for finite and infinite dimensional systems," *SIAM J. Control Optim.*, vol. 48, no. 2, pp. 1206–1228, 2009.

[30] M. Reble and F. Allgöwer, "Unconstrained model predictive control and suboptimality estimates for nonlinear continuous-time systems," *Automatica*, vol. 48, no. 8, pp. 1812–1817, 2012.

[31] P. Tøndel, T. A. Johansen, and A. Bemporad, "Evaluation of piecewise affine control via binary search tree," *Automatica*, vol. 39, no. 5, pp. 945–950, 2003.

[32] T. Goggia *et al.*, "Integral sliding mode for the torque-vectoring control of fully electric vehicles: Theoretical design and experimental assessment," *IEEE Trans. Veh. Technol.*, vol. 64, no. 5, pp. 1701–1715, May 2015.

[33] H. B. Pacejka, *Tire and Vehicle Dynamics*. Oxford, U.K.: Butterworth, 2012.

[34] T. Geyer, F. D. Torrisi, and M. Morari, "Optimal complexity reduction of polyhedral piecewise affine systems," *Automatica*, vol. 44, pp. 1728–1740, Jul. 2008.

[35] M. S. Santina and A. R. Stubberud, *Basics of Sampling and Quantization. Handbook of Networked and Embedded Control Systems*. Boston, MA, USA: Birkhäuser, 2005.

[36] J. H. Park and C. Y. Kim, "Wheel slip control in traction control system for vehicle stability," *Veh. Syst. Dyn.*, vol. 31, no. 4, pp. 263–278, 1999.

[37] R. W. Allen, T. J. Rosenthal, and J. P. Chrstos, "A vehicle dynamics tire model for both pavement and off-road conditions," SAE Tech. Paper 970559, 1997.
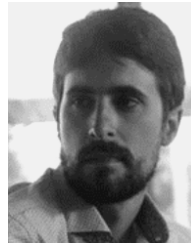
**Davide Tavernini** received the M.Sc. degree in mechanical engineering and the Ph.D. in dynamics and design of mechanical systems from the University of Padova, Padua, Italy, in 2010 and 2014, respectively. During his Ph.D. he was with the Motorcycle Dynamics Research Group.

He is currently a Lecturer in advanced vehicle engineering with the University of Surrey, Guildford, U.K. His current research interests include vehicle dynamics modeling and control, mostly applied to electric and hybrid vehicles.

**Mathias Metzler** (GS'17) received the Dipl.-Ing. degree (*summa cum laude*) in mechanical engineering from the Vienna University of Technology, Vienna, Austria, in 2015. He is currently pursuing the Ph.D. degree in advanced vehicle engineering with the University of Surrey, Guildford, U.K.

His current research interests include vehicle dynamics control, model predictive control, optimization, and nonlinear systems.

**Patrick Gruber** received the M.Sc. degree in motorsport engineering and management from Cranfield University, Cranfield, U.K., in 2005, and the Ph.D. degree in mechanical engineering from the University of Surrey, Guildford, U.K., in 2009.

He is currently a Senior Lecturer in advanced vehicle systems engineering with the University of Surrey. His current research interests include vehicle dynamics and tire dynamics with special focus on friction behavior.

**Aldo Sorniotti** (M'12) received the M.Sc. degree in mechanical engineering and Ph.D. degree in applied mechanics from the Politecnico di Torino, Turin, Italy, in 2001 and 2005, respectively.

He is currently a Professor in advanced vehicle engineering with the University of Surrey, Guildford, U.K., where he coordinates the Centre for Automotive Engineering. His current research interests include vehicle dynamics control and transmission systems for electric and hybrid vehicles.